

# Space Charge Influence on the Angle of Conical Spikes Developing on a Liquid-Metal Anode

G. Sh. Boltachev,<sup>\*</sup> N. M. Zubarev,<sup>†</sup> and O. V. Zubareva<sup>‡</sup>  
*Institute of Electrophysics, Ural Division, Russian Academy of Sciences,  
106 Amundsen Street, 620016 Ekaterinburg, Russia*

The influence of the space charge of ions emitted from the surface of a conical spike on its shape has been studied. The problem of the calculation of the spatial distributions of the electric field, ion velocity field, and the space charge density near the cone tip has been reduced to the analysis of a system of ordinary differential equations. As a result of numerical solution of these equations, the criterion of the balance of the capillary and electrostatic forces on the conic surface of a liquid-metal anode has been determined. It has allowed us to relate the electrical current flowing through the system, the applied potential difference and the cone angle. We have compared the results of our calculations with available experimental data concerning emission from the surface of pure liquid gallium (Ga), indium (In), tin (Sn), and some liquid alloys, such as Au+Si, Co+Ge, and Au+Ge. On the basis of the proposed model, explanations have been given for a number of specific features of the emissive behavior of different systems.

PACS numbers: 41.20.Cv, 52.59.Sa

## Introduction

It is known that, as a result of the electrohydrodynamic instability development, the surface of a conducting liquid (liquid metal) takes the shape of a cone in a rather strong external electric field [1–7]. An enhancement of the field near the cone tip provides conditions for the initiation of emission processes such as field evaporation of ions [8–12]. Interest in studying the geometry of such structures was stimulated in large measure by the development of liquid-metal ion sources (LMIS). Considerable progress in the theory of conical spikes started from Taylor's investigations [2, 13]. He has shown that, for a cone with a half-angle of  $\alpha_T \simeq 49.3^\circ$ , the surface electrostatic pressure  $P_E$  depends on the distance from its apex as  $R^{-1}$  and, hence, can be counterbalanced by the surface pressure  $P_L \sim R^{-1}$ .

The geometry of ion-emitting cones (Taylor cones) was investigated in numerous experimental works [14–19]. These works testify that an increase in the applied potential difference is accompanied not only by the appearance and increase of the emission current, but also by a decrease of the cone half-angle. For small currents, i.e., when the space charge influence is negligible, the half-angle is close to Taylor's angle  $\alpha_T$ . The phenomenon of a cone sharpening can be interpreted as the system response aimed at the conservation of the balance of the pressures  $P_E$  and  $P_L$  under the conditions of the screening effect of the space charge. The last effect in case of an emitter with invariable shape, as is known [20, 21], reduces to the Child-Langmuir law.

Simple analytic models, which relate the basic param-

eters of a problem, play an important role in gaining an insight into the physical processes that occur in liquid-metal ion sources. Among these models are Mair's theory [22], the models by Kingham & Swanson [10], Mair & Forbes [23, 24], and, certainly, Taylor's model [2]. Nevertheless, the above-listed models do not present a theoretical description of the current dependence of the cone angle. In this work, we propose a model, which generalizes, on the one hand, Taylor's solution to the case where the space charge starts playing an important part, and on the other hand, the Child-Langmuir law to the case of an emitter of variable (self-adjusting) shape. It is based on self-similar solutions for a charged particle flow [25, 26], which were found to be compatible with the Laplace-Young stress condition for a liquid conducting cone: see our Letter [27]. Clearly, this model does not attempt to describe all the features of operation of liquid-metal ion sources. The application of self-similar solutions restricts our analysis to precisely conical shape of the emitter. So, possible deformations of the emitting cone observed in experiments, in particular, the appearance of small jet-like protrusion on its vertex remain beyond the scope of this paper. The advantage of the proposed model is the possibility to describe distributions of the electric field potential and of the ion velocity field over the cone and, as a consequence, to obtain relations between the cone angle, the current, and the applied voltage.

## I. INITIAL EQUATIONS; SELF-SIMILAR REDUCTION

Let us consider a single-velocity flow of ions evaporating from the surface of an infinite conical anode in the framework of the hydrodynamic description [25–28]. Figure 1 shows the geometry of the problem and the notations used. The mass and charge densities are proportional to each other for a charged-particle flow, and

<sup>\*</sup>Electronic address: grey@iep.uran.ru

<sup>†</sup>Electronic address: nick@ami.uran.ru

<sup>‡</sup>Electronic address: olga@ami.uran.ru

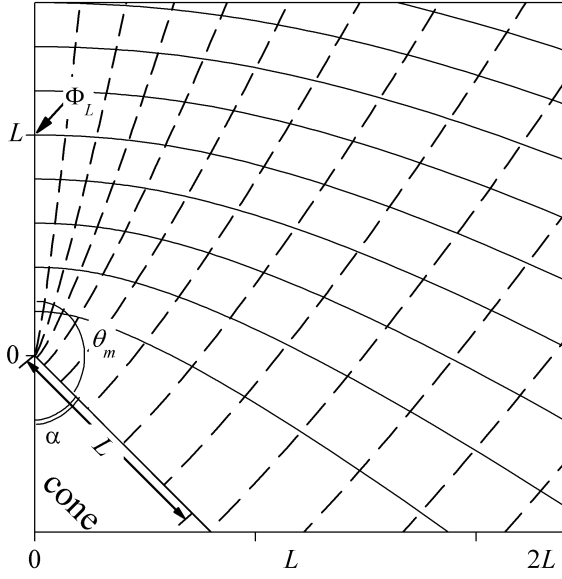


FIG. 1: The geometry of the problem and the notations:  $L$  is the characteristic spatial scale,  $\alpha$  is the cone half-angle,  $\theta_m \equiv \pi - \alpha$ ,  $\Phi_L$  is the absolute value of electric field potential at the symmetry axis at the distance  $L$  from the apex of the cone. The solid lines correspond to the equipotential surfaces, including the surface of the cone with  $\Phi = 0$ . The dashed lines correspond to the streamlines of the ion flow.

vorticity of the flow is conserved in a potential electric field ( $\mathbf{E} = -\nabla\Phi$ ). We assume the initial ion velocity to be equal to zero. This approximation can be considered to be well founded in view of the extremely high values of electric field strength near the cone tip. Then the vorticity of the flow is zero close to the anode surface, and, hence, the ion flow is potential. In this case, the flow velocity, along with the electric field, can be described with the help of a scalar function, the velocity potential:  $\mathbf{v} = \nabla\Psi$ . Then the original set of equations can be written as follows:

$$\nabla^2\Phi = -qN/\varepsilon_0, \quad (1)$$

$$m(\nabla\Psi)^2/2 = -q\Phi, \quad (2)$$

$$\nabla(N\nabla\Psi) = 0. \quad (3)$$

The first equation is the Poisson equation for the electric field potential  $\Phi$ ; here  $N$  is the charged particle density,  $q$  is the particle charge, and  $\varepsilon_0$  is the vacuum permittivity. The motion of particles is described by the second equation, which gives the energy conservation law for ions in an electric field ( $\Psi$  is the velocity potential,  $m$  is the mass of a particle). The third equation is the continuity equation. The Poisson equation (1) has to be solved together with the condition that the conductor surface is equipotential. It is convenient to take the electric potential of the the anode be equal to zero,  $\Phi = 0$ , which agrees with the condition that the initial velocity of particles is zero,  $\nabla\Psi = 0$  (see equation (2)).

The equilibrium configuration of the free liquid-metal surface is determined by the balance condition for the

electrostatic and capillary forces (the Laplace-Young equation). For a conical surface it takes the form:

$$P_L = \frac{\sigma}{R} \cot \alpha = \frac{\varepsilon_0}{2} (\nabla\Phi)_{\Phi=0}^2 = P_E, \quad (4)$$

where  $\alpha$  is the cone half-angle,  $\sigma$  is the surface tension, and  $R$  is the distance from the cone apex. In the case of a high mass flow rate, characteristic for the so-called cone-jet mode of electrospays [29, 30] or for sonic sprays [31], the hydrodynamic term also contributes to the pressure balance condition. However, for the process of field evaporation of ions realized in the experiments [14–19], this term appears to be 2–3 orders of magnitude less than the electrostatic ( $P_E$ ) and capillary ( $P_L$ ) terms [3], and we can neglect it.

In order to pass to dimensionless variables, we introduce some characteristic spatial scale  $L$ , which will be taken as the unit of length (see Fig. 1). Since the equations (1)–(3) have no their own characteristic spatial size (they are invariant with respect to scaling), the value of  $L$  cannot be defined from the model. Below we will treat  $L$  as a size of the top part of an infinite model cone; the emission current from this part of the cone will be identified with the experimental current from a liquid-metal ion source. As an external control parameter, we introduce the absolute value of electric field potential at the symmetry axis at the same distance  $L$  from the apex of the cone,  $\Phi_L > 0$ . Then it is convenient to define the dimensionless variables by the following way:

$$r = R/L, \quad \phi = -\Phi/\Phi_L, \quad (5)$$

$$n = NL^2q/(\varepsilon_0\Phi_L), \quad \psi = \Psi [m/(2qL^2\Phi_L)]^{1/2},$$

and the initial equations (1)–(3) takes the form:

$$\nabla^2\phi = n, \quad (\nabla\psi)^2 = \phi, \quad \nabla(n\nabla\psi) = 0. \quad (6)$$

Switching to spherical coordinates and taking into consideration the axial symmetry of the problem, we obtain:

$$\begin{aligned} \phi_{rr} + \frac{2}{r}\phi_r + \frac{1}{r^2}\phi_{\theta\theta} + \frac{\cot\theta}{r^2}\phi_\theta &= n, \\ \psi_r^2 + \frac{1}{r^2}\psi_\theta^2 &= \phi, \\ n_r\psi_r + \frac{n_\theta\psi_\theta}{r^2} + n \left[ \psi_{rr} + \frac{2}{r}\psi_r + \frac{\psi_{\theta\theta}}{r^2} + \frac{\cot\theta}{r^2}\psi_\theta \right] &= 0. \end{aligned} \quad (7)$$

It can readily be seen that these equations are invariant under the scale transformations

$$\begin{aligned} \phi &\rightarrow \phi \cdot s^\gamma, & n &\rightarrow n \cdot s^{\gamma-2}, \\ \psi &\rightarrow \psi \cdot s^{\gamma/2+1}, & r &\rightarrow r \cdot s, \end{aligned} \quad (8)$$

where  $\gamma$  and  $s$  are some constants. Consequently, the system (7) can be reduced by means of the following self-similar ansatz (see also [25, 26]):

$$\phi = r^\gamma A(\theta), \quad n = r^{\gamma-2} B(\theta), \quad \psi = r^{\gamma/2+1} C(\theta), \quad (9)$$

where  $A$ ,  $B$ , and  $C$  are unknown functions of the polar angle  $\theta$ .

In the dimensionless form, the pressure balance condition (4) reads

$$(\nabla\phi)_{\phi=0}^2 = \frac{\cot\alpha}{rV^2}, \quad V \equiv \Phi_L \sqrt{\frac{\varepsilon_0}{2L\sigma}}. \quad (10)$$

The dimensionless group  $V$  plays the role of an external control parameter of the problem. One can see from this expression that the electric potential has to depend on the distance  $r$  as  $\phi \sim r^{1/2}$  that uniquely determines the value of the self-similarity parameter:  $\gamma = 1/2$  [2, 13]. Thus, we should apply the substitution

$$\begin{aligned} \phi(r, \theta) &= r^{1/2}A(\theta), \\ n(r, \theta) &= r^{-3/2}B(\theta), \\ \psi(r, \theta) &= r^{5/4}C(\theta), \end{aligned} \quad (11)$$

which provides separation of variables in (7). The substitution (11) enables us to reduce the partial differential equations (7) to the following set of second-order ordinary differential equations for the angle distribution of  $A(\theta)$ ,  $B(\theta)$  and  $C(\theta)$ :

$$\begin{aligned} (3/4)A + A_{\theta\theta} + A_{\theta} \cot\theta &= B, \\ (25/16)C^2 + C_{\theta}^2 &= A, \\ (15/16)BC + B_{\theta}C_{\theta} + BC_{\theta\theta} + BC_{\theta} \cot\theta &= 0. \end{aligned} \quad (12)$$

Note that the last equation can be simplified by introducing an auxiliary function  $D(\theta) \equiv BC_{\theta} \sin\theta$ :

$$D_{\theta}C_{\theta} = -(15/16)DC. \quad (13)$$

Solutions of Eqs. (12) must satisfy a number of conditions at the symmetry axis ( $\theta = 0$ ) and on the cone surface ( $\theta = \theta_m \equiv \pi - \alpha$ ):

$$A(0) = 1, \quad C_{\theta}(0) = 0, \quad A(\theta_m) = 0. \quad (14)$$

Note that the condition that the initial velocities of emitted particles are equal to zero, i.e., the pair of conditions  $C(\theta_m) = 0$  and  $C_{\theta}(\theta_m) = 0$ , follows from the second equation of the set (12). Differentiating the same equation with respect to  $\theta$ , we find that the condition  $A_{\theta}(0) = 0$  is satisfied if the second derivative of the function  $C(\theta)$  is finite at the symmetry axis. So, the solution of the problem (12) and (14) is unique for a given value of  $\theta_m$ .

The additional boundary condition

$$A_{\theta}(\theta_m) = -V^{-1}\sqrt{\cot\alpha}, \quad (15)$$

resulting from the pressure balance condition (10), is not used in seeking a solution of Eqs. (12). It allows us to determine the value of the parameter  $V$  that corresponds to the angle  $\theta_m$ . Now, let us rewrite this condition in the following form:

$$V = \sqrt{\cot\alpha}/E(\alpha), \quad E(\alpha) \equiv -A_{\theta}(\theta_m). \quad (16)$$

The function  $E(\alpha)$  defines the dimensionless value of the electric field strength on the cone surface at a distance  $r = 1$  from the apex ( $E(\alpha) = |\nabla\phi|_{r=1, \theta=\theta_m}$ ).

The intensity of the ion flux can be characterized by the electrical current  $I$  (in dimensional form) flowing through the sphere of radius  $L$  with a center at the apex of the cone:

$$I = 2\pi qL^2 \int_0^{\theta_m} N\Psi_R \sin\theta d\theta. \quad (17)$$

As a corresponding dimensionless quantity, it is convenient to take the group

$$J \equiv I \frac{\sqrt{m}}{(32q^2\varepsilon_0L^3\sigma^3)^{1/4}}, \quad (18)$$

which does not contain the potential difference  $\Phi_L$ . It can be expressed in terms of the functions  $B$  and  $C$  by following relation:

$$J = V^{3/2}F(\alpha), \quad F(\alpha) \equiv \frac{5\pi}{2} \int_0^{\theta_m} BC \sin\theta d\theta. \quad (19)$$

The function  $F(\alpha)$  defines the particle flux from the top part of the cone,  $0 < r < 1$ .

The self-similar solutions (11) give the ion flux density ( $j \sim n|\nabla\psi|$ ) and the electric field intensity ( $|\nabla\phi|$ ) proportional to  $r^{-5/4}$  and, respectively, to  $r^{-1/2}$ . This corresponds to the power law between the quantities  $j$  and  $|\nabla\phi|$  on the cone surface,

$$j \sim |\nabla\phi|^{5/2}. \quad (20)$$

It correctly reflects the basic property of the system, namely, the nonlinear growth of current density with increasing intensity. Nevertheless, the 5/2 power law certainly differs from the exponential dependence determined by the kinetics of the field evaporation process [32].

Our solutions would be exact if the actual relation between the flux density and the electric field were the same as the model relation (20). Note that the self-similar solutions corresponding to the model law of emission (20) are the only solutions consistent with our main assumption that the surface of a liquid metal is conical. Any distinction of the law of emission from the model law (20) will lead to deviation of the surface from the ideal cone.

However, it is known from the experiments [14–19] that the surface takes a near-conical shape, and it is possible to associate it with a certain cone half-angle  $\alpha$  (the method of angle measurement is given in the above-mentioned papers). That is, the details of the current density distribution over the emitter surface (basically, ions evaporate from the protrusion growing at the cone apex) have a relatively small influence on the balance between the electrostatic and capillary forces at the periphery of the cone structures. The reason is that the

influence of the space charge has an integral character (this phenomenon is most conspicuous in planar geometry, where the screening effect of the space charge in principle does not depend on its distribution). As a consequence, our approach, not claiming to describe LMIS operation in detail, is rather applicable for the analysis of the integral (averaged) characteristics of LMIS, including the relations between the cone half-angle  $\alpha$ , the total emission current  $J$ , and the applied voltage  $V$ . The relations between these main model parameters is determined by the expressions (16) and (19). In the next section, the set of Eqs. (12) will be solved numerically. It will allow us to find the auxiliary functions  $E(\alpha)$  and  $F(\alpha)$ , which appeared in (16) and (19). As a consequence, the dependence of  $\alpha$  on  $J$  ( $V$  plays the role of the parameter) and the current-voltage dependence ( $\alpha$  is the parameter) will be established.

## II. CONSTRUCTION OF SOLUTIONS

### A. Asymptotic expansions

In order to solve the ordinary differential equations (12) and (13) with the conditions (14) numerically, we should use asymptotic expansions for the unknown functions at  $\theta \rightarrow 0$  and  $\theta \rightarrow \theta_m$ . This is caused by the singular behavior of the functions (or their derivatives) at the boundaries  $\theta = 0$  and  $\theta = \theta_m$ . As will be shown below,  $B \rightarrow \infty$  at  $\theta \rightarrow \theta_m$  and  $B_{\theta\theta\theta} \rightarrow \infty$  at  $\theta \rightarrow 0$ .

At  $\theta \rightarrow 0$ , i.e., at the symmetry axis, the functions  $A(\theta)$ ,  $B(\theta)$ ,  $C(\theta)$ , and  $D(\theta)$  can be expanded into the series

$$\begin{aligned} A &= 1 + a_2\theta^2 + a_4\theta^4 + \dots, \\ B &= b_0\theta^\beta + b_0b_1\theta^{2+\beta} + \dots, \\ C &= 4/5 + c_2\theta^2 + c_4\theta^4 + \dots, \\ D &= d_0\theta^{2+\beta} + d_0d_2\theta^{4+\beta} + \dots \end{aligned} \quad (21)$$

Substitution of these expressions into the initial equations (12), (13) yields

$$\begin{aligned} a_2 &= -\frac{3}{24}, & a_4 &= \frac{1}{210}, & \dots, \\ c_2 &= \frac{-5 + \sqrt{13}}{24}, & c_4 &= \frac{295 - 107\sqrt{13}}{9 \cdot 2^{10}}, & \dots, \\ \beta &= \frac{\sqrt{13} + 1}{2} \simeq 2.3, & b_1 &= -\frac{275 + 173\sqrt{13}}{1152}, & \dots, \\ d_0 &= 2b_0c_2, & d_2 &= -\frac{165 + 31\sqrt{13}}{384}, & \dots \end{aligned} \quad (22)$$

The expansions (21) satisfy two first conditions from (14); they contain a free parameter (the coefficient  $b_0$ ), which is determined by the following condition at the cone surface:  $A(\theta_m) = 0$ . Note that the divergence of higher derivatives of the function  $B$  leads to the divergence of higher derivatives of the functions  $A$  and  $C$ . The next

terms of the expansions (21) for  $A$  and  $C$  are of the order of  $\theta^{2+\beta}$ .

In the limit  $\theta \rightarrow \theta_m$ , i.e., on the cone surface, the unknown functions can be expanded into power series in the parameter  $x = \theta_m - \theta$ :

$$\begin{aligned} A &= x^{1/2} \sum_{i=1} a'_i x^{i/2}, & B &= x^{-1} \sum_{i=1} b'_i x^{i/2}, \\ C &= x \sum_{i=1} c'_i x^{i/2}, & D &= d'_0 \left( 1 + x^{3/2} \sum_{i=1} d'_i x^{i/2} \right). \end{aligned} \quad (23)$$

The first coefficients of these expansions are listed below:

$$\begin{aligned} a'_2 &= \frac{4}{3} b'_1, & c'_1 &= \frac{2}{3} \sqrt{a'_1}, \\ c'_2 &= \frac{1}{3} \frac{b'_1}{\sqrt{a'_1}}, & b'_2 &= -\frac{2}{3} \frac{b'_1{}^2}{a'_1}, \\ d'_0 &= -b'_1 \sqrt{a'_1} \sin \theta_m, & d'_1 &= -\frac{5}{16}. \end{aligned} \quad (24)$$

Free parameters of these expansions, namely, the coefficients  $a'_1$  and  $b'_1$ , are determined by the boundary conditions at the symmetry axis.

Increasing the charge density over the cone leads to screening of the electric field at its surface, i.e., the coefficient  $a'_1$  will approach zero. In the formal limit  $a'_1 = 0$  (the electric field turns to zero at the anode surface), another asymptotics is realized:

$$\begin{aligned} A &= x^{1/3} \sum_{i=1} a''_i x^i, & B &= x^{-5/3} \sum_{i=1} b''_i x^i, \\ C &= x^{2/3} \sum_{i=1} c''_i x^i, & D &= d''_0 \left( 1 + x \sum_{i=1} d''_i x^i \right), \end{aligned} \quad (25)$$

where

$$\begin{aligned} a''_1 &= \frac{9}{4} b''_1, & a''_2 &= \frac{6}{5} b''_1 \cot \theta_c, \\ c''_1 &= \frac{9}{10} \sqrt{b''_1}, & c''_2 &= \frac{3}{20} \sqrt{b''_1} \cot \theta_c, \\ b''_2 &= \frac{11}{15} b''_1 \cot \theta_c, & d''_0 &= -\frac{3}{2} b''_1{}^{3/2} \sin \theta_c, \\ d''_1 &= -\frac{9}{32}, & \dots &. \end{aligned} \quad (26)$$

These expressions contain two free parameters: the coefficient  $b''_1$  (or  $d''_0$ ) and the angle  $\theta_m \equiv \theta_c$  at which complete screening of the external field occurs.

It should be noted that the function  $D$  converges rapidly near the cone surface for both forms of expansion, (23) and (25). Therefore, using the function  $D$  is preferable to using the function  $B$  in the procedure of numerical integration of the problem (12)–(14).

### B. Numerical calculations

The set of Eqs. (12), (13) was solved numerically by the prediction-correction method of the third order. The

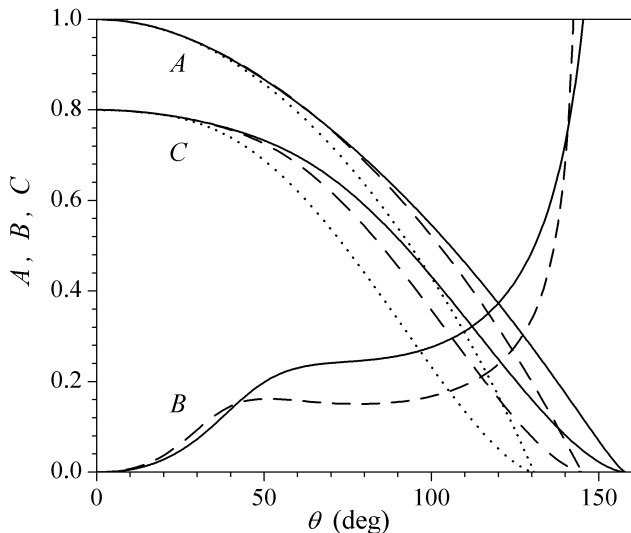


FIG. 2: Solutions of the system (12) for the cone half-angles  $\alpha = \alpha_T$  (in this case,  $B \equiv 0$ ) (dotted lines),  $\alpha = 35^\circ$  (dashed lines), and  $\alpha = \alpha_c$  (solid lines).

calculation starts from the asymptotics (23) or (25). It has been found that the equations admit solutions for the angles in the range  $\theta_T \leq \theta_m \leq \theta_c$ . The minimum angle value  $\theta_T \simeq 130.71^\circ$  corresponds to the Taylor cone ( $\alpha = \alpha_T \simeq 49.29^\circ$ ) and refers to the special case of no space charge, i.e.,  $B = 0$ . For this case, the  $\theta$  dependence of  $A$  is determined by the Legendre function  $P_{1/2}(\cos \theta)$ . The upper bound of the angle,  $\theta_c$ , equals  $\simeq 158.11^\circ$ . It corresponds to the least possible half-angle of the cone  $\alpha = \alpha_c \simeq 21.89^\circ$ . This configuration of the surface relates to the formal limit that the electric field at the cone is completely screened by the space charge (this limit cannot be achieved because of the finite emissivity of the surface). The results of the calculations, corresponding to different values of  $\alpha$ , are presented in Fig. 2. In view of the obvious relations

$$\begin{aligned} \nabla\phi &= r^{-1/2} \{A/2, A_\theta, 0\}, \\ \nabla\psi &= r^{1/4} \{5C/4, C_\theta, 0\}, \end{aligned} \quad (27)$$

the angle dependence of  $A(\theta)$  and  $C(\theta)$  give an idea of the distributions of the electric field and the velocity field. As an example, Fig. 1 shows the equipotential surfaces and streamlines of the flow corresponding to  $\alpha = 45^\circ$ .

### C. The electric field strength at the cone surface

The calculations show that the function  $E(\alpha)$  grows monotonically from zero to the value  $\simeq 0.975$  as the angle  $\alpha$  increases from  $\alpha_c$  to  $\alpha_T$  (see Fig. 3). Near the limiting case (25), the estimate  $E(\alpha) \sim (\alpha - \alpha_c)^{1/2}$  is valid for  $\alpha \rightarrow \alpha_c$ . To verify this dependence, it is possible to draw an analogy between the considered problem and the problem of a charged-particle flow in a plane vacuum

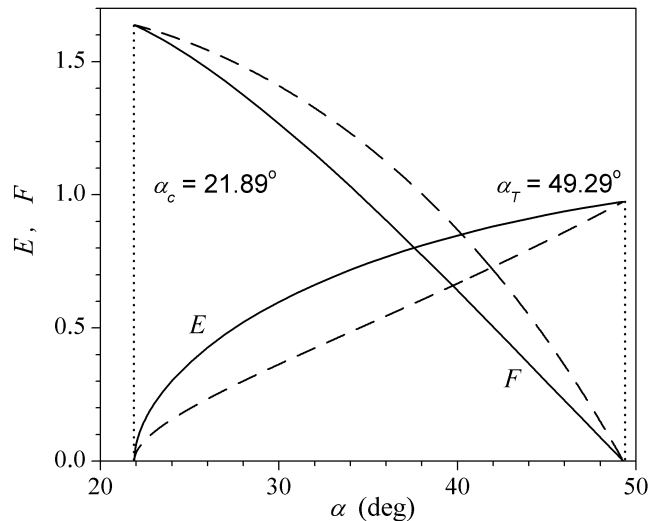


FIG. 3: The auxiliary functions  $E(\alpha)$  and  $F(\alpha)$  (solid lines), which represent the electric field strength on the cone surface at  $r = 1$  and, respectively, the ion flux from the top part of the cone ( $0 < r < 1$ ). The dashed lines correspond to the one-dimensional model (Eqs. (31)–(33)).

diode, which can be solved analytically. Actually, in the one-dimensional case, where all quantities depend only on one coordinate  $z$ , the equations (6) reduce to the set of ordinary differential equations

$$\phi_{zz} = n, \quad \psi_z^2 = \phi, \quad (n\psi_z)_z = 0, \quad (28)$$

which look like the equations (12) after the substitution  $z \rightarrow \theta$ . These equations admit the following exact implicit solution for the electric field potential  $\phi$ :

$$6j^2z - E_0^3 = \left(2j\sqrt{\phi} - E_0^2\right) \sqrt{4j\sqrt{\phi} + E_0^2}, \quad (29)$$

where  $j = n\psi_z$  is the constant current density,  $E_0 = \phi_z|_{z=0}$  is the electric field strength at the planar emitter. Let us also introduce the notation for the electric strength at the opposite electrode,  $E_1 = \phi_z|_{z=h}$ , ( $h$  is the interelectrode distance) and for the electric potential on it,  $\phi_h = \phi|_{z=h}$ . From the solution (29) one can obtain the relations between the quantities  $E_0$ ,  $E_1$ ,  $\phi_h$ ,  $h$ , and  $j$ ,

$$\begin{aligned} 4j\sqrt{\phi_h} &= E_1^2 - E_0^2, \\ 6j^2h - E_0^3 &= \left(2j\sqrt{\phi_h} - E_0^2\right) E_1. \end{aligned} \quad (30)$$

By analogy with  $\theta_c$ , we introduce the interelectrode distance  $h_c = 4\phi_h/(3E_1)$ , corresponding to the limit  $E_0 = 0$ , and then rewrite the expressions (30) as

$$j = \frac{4\phi_h^{3/2}}{9h_c^2} \left(1 - \frac{E_0^2}{E_1^2}\right), \quad \frac{h}{h_c} = 1 - \left(\frac{E_0}{E_1 + E_0}\right)^2. \quad (31)$$

Note that, in the limit  $E_0/E_1 \rightarrow 0$ , the first equation of (31) represents the Child-Langmuir law [20, 21] for a

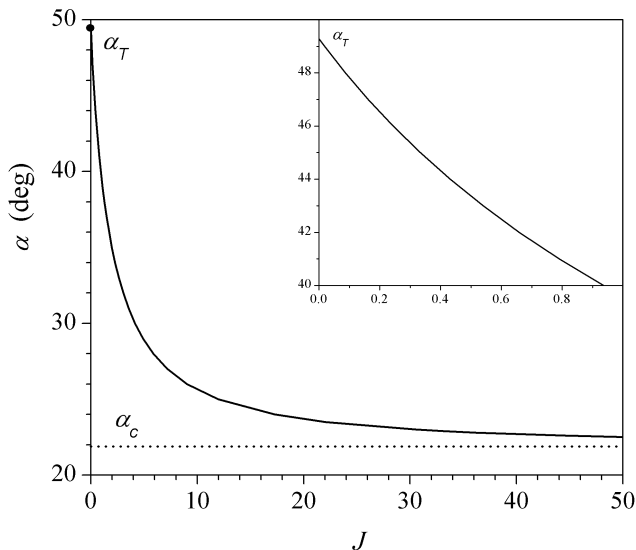


FIG. 4: Dependence of the cone half-angle  $\alpha$  on the dimensionless emission current  $J$ . The inset demonstrates the same dependence for relatively small currents.

plane vacuum diode. It follows from the second equation of (31) that  $E_0 \approx E_1 \sqrt{1 - h/h_c}$  in the same limit, i.e., for fixed  $\phi_h$  and  $E_1$ , the electric field strength at the emitter surface  $E_0$  has a square root dependence on the small quantity  $h_c - h$ . For  $h = h_c$ , the electric field at the emitter surface is completely screened by the space charge. At given  $\phi_h$  and  $E_1$ , the space charge density decreases as the interelectrode distance  $h$  is reduced. The opposite limit, where the space charge is absent ( $E_0 = E_1$  and  $\phi(z) = E_1 z$ ), is reached at  $h = (3/4)h_c$ .

So, in the framework of the discussed analogy we can identify (i) the angles  $\theta_m$ ,  $\theta_c$ , and  $\theta_T$  with the interelectrode distances  $h$ ,  $h_c$ , and  $h_T = (3/4)h_c$ , respectively, (ii) the electric field strength on the cone surface at a unit distance from the apex  $E$  with the strength at the surface of the planar emitter surface  $E_0$ , (iii) the electric field strength at the symmetry axis at a unit distance from the cone apex  $|\nabla\phi| = 1/2$  with the strength at the opposite electrode  $E_1$ , and also (iv) unit potential difference between the cone axis and its surface for  $r = 1$  with the fixed potential difference  $\phi_h$  for a plane vacuum diode. In order to compare the characteristics of conical and planar diodes, we apply the linear mapping of the angle interval  $\theta_T \leq \theta_m \leq \theta_c$  into the interval of distances  $h_T \leq h \leq h_c$ ,

$$\frac{h - h_T}{h - h_c} = \frac{\theta_m - \theta_c}{\theta_m - \theta_T}. \quad (32)$$

The analogs of the functions  $F(\alpha)$  and  $E(\alpha)$  corresponding to the one-dimensional model (28),

$$F_{pl} = \frac{9j h_c^2}{4\phi_h^{3/2}} F(\alpha_c), \quad E_{pl} = \frac{E_0}{E_1} E(\alpha_T), \quad (33)$$

are presented in Fig. 3. It can be seen that the properties

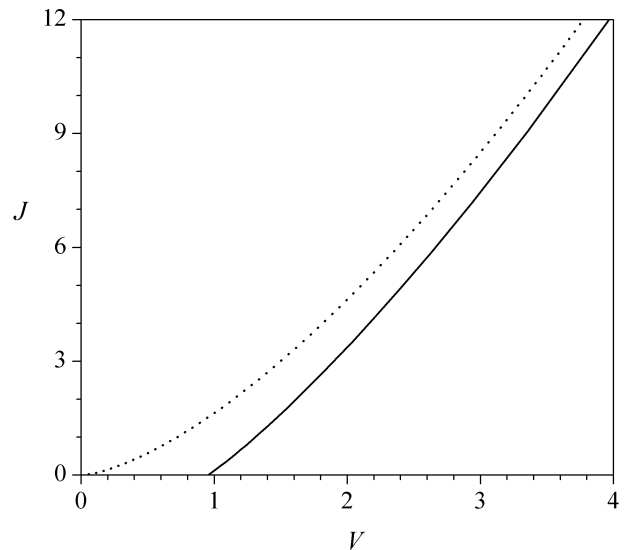


FIG. 5: The current  $J$  as a function of the applied potential difference  $V$ . The dotted line shows the asymptotic shape of the current-voltage characteristic corresponding to the Child-Langmuir law.

of conical (12) and planar (28) models are qualitatively similar. Consequently, we should expect that  $E \sim (\theta_c - \theta_m)^{1/2}$  at  $\theta_m \rightarrow \theta_c$ , or, in terms of the cone half-angle,  $E \sim (\alpha - \alpha_c)^{1/2}$  at  $\alpha \rightarrow \alpha_c$ , as we wished to show.

Taking into account such a dependence near the limiting regime (25), we approximate the calculated dependence of  $E$  on  $\alpha$ , by the formula

$$E(\alpha) = -0.9754 \xi - 0.6176 \xi^2 + 0.8342 \xi^3 - 0.2164 \xi^4, \quad (34)$$

where  $\xi = [(\alpha - \alpha_c)/(\alpha_T - \alpha_c)]^{1/2}$ . The error of the approximation (34) is less than 0.1% over the range  $\alpha_c < \alpha < \alpha_T$ . According to the balance condition (16), the obtained dependence  $E(\alpha)$  determines the relation between geometry of the emitting cusp, i.e., the angle  $\alpha$ , and the external control parameter of the system, i.e., the potential  $V \sim \Phi_L$ .

#### D. The relations between model parameters

The quantity  $F(\alpha)$ , which is determined by (19), specifies a particle flux from the top part of the cone,  $0 < r < 1$ . The angular dependence of this function obtained as a result of numerical solution of the problem (12)–(14) is presented in Fig. 3. The calculated function  $F(\alpha)$  can be approximated by the relation

$$F(\alpha) \simeq 1.8863\zeta + 0.0956\zeta^2 - 0.2259\zeta^3 - 0.1167\zeta^4, \quad (35)$$

where  $\zeta(\alpha) = 1 - \xi^2 = (\alpha_T - \alpha)/(\alpha_T - \alpha_c)$ . The error of this approximation is less than 0.15%. Note that the function  $F(\alpha)$  monotonically decreases from  $\simeq 1.637$  to zero as the angle  $\alpha$  changes from  $\alpha_c$  to  $\alpha_T$ .

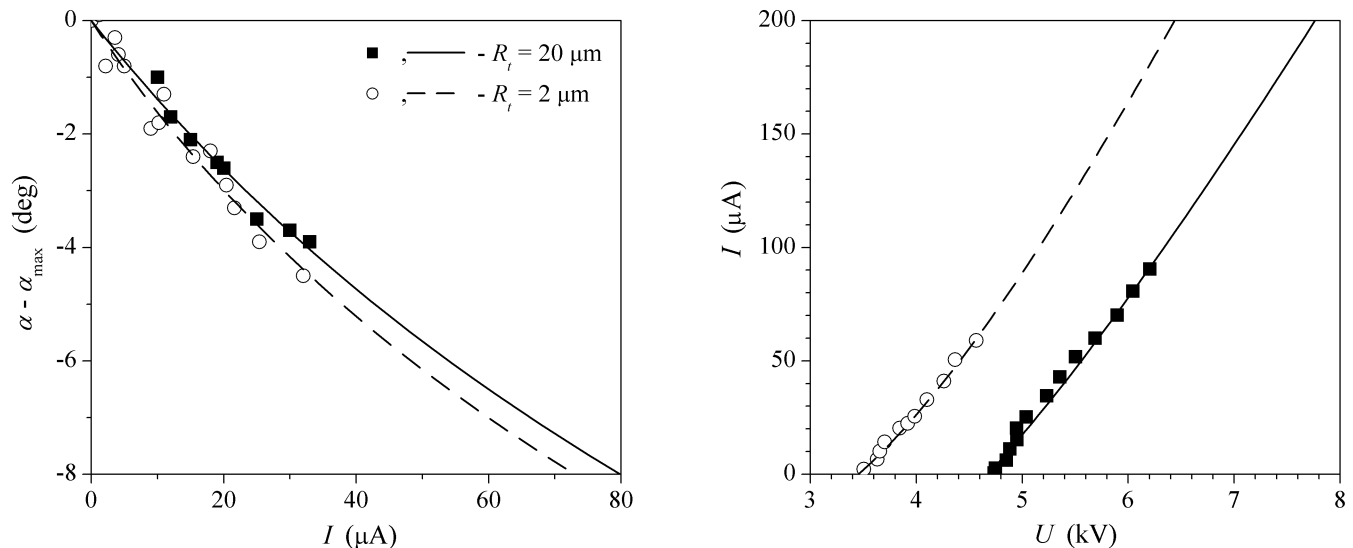


FIG. 6: The change in the cone half-angle versus the emission current (left) and the current-voltage characteristics (right) for a gallium liquid-metal ion source. The points correspond to the experimental data of [15] and the lines to the theory.

The expressions (16) and (19) together with (34) and (35) allow us to obtain the dependence of the cone half-angle  $\alpha$  on the current  $J$  as well as the current-voltage characteristic of the cone, i.e., the dependence of  $J$  on  $V$ . These relationships are plotted in Figs. 4 and 5, respectively.

From Fig. 4 it can be seen that the angle monotonically decreases with increasing current. It is equal to the Taylor angle  $\alpha_T \approx 49.29^\circ$  at zero current and tends to the angle  $\alpha_c \approx 21.89^\circ$  in the formal limit of an infinite current. Note that the interpretation of experiments [14–19] in the framework of our model corresponds to the dimensionless current in the range  $0 < J < 1$  (see the inset of Fig. 4). For larger current values, the cone structure becomes unstable.

An important feature of the theoretical current-voltage characteristic (Fig. 5) is its threshold character. There is no electric current,  $J = 0$ , if  $V < V_0 = \sqrt{\text{ctg } \alpha_T} / f(\alpha_T) \simeq 0.9512$ . This is related to the impossibility of a balance between the electrostatic and capillary forces at a relatively small potential difference. The capillary force will dominate and the cone structure will break. In the formal limit of large  $V$  the model yields the universal Child-Langmuir law:  $J \rightarrow F(\alpha_c)V^{3/2}$ , which describes the regime of space-charge limitation of the current as a result of complete screening of the electric field at the electrode surface.

Excluding the parameter  $\alpha$  from (16) and (19), we can rewrite the dependence of  $J$  on  $V$  in the explicit form. The function  $F$  linearly goes up to the value  $F(\alpha_c)$  as  $\alpha \rightarrow \alpha_c$  (see Fig. 3), and, as discussed above, the function  $E$  tends to zero according to the square root law. As a consequence, the dependence of  $J$  on  $V$  must have the form  $J \approx j_0 V^{3/2} + j_1 V^{-1/2}$  in the limit  $V \rightarrow \infty$ . With this estimate taken into account, for  $V > V_0$  the required

dependence can be approximated by the expression

$$J = V^{3/2} \left( j_0 + \frac{j_1}{V^2} + \frac{j_2}{V^4} + \frac{j_3}{V^6} \right). \quad (36)$$

The coefficients of the approximation (36) are the following:  $j_0 = 1.6372$ ,  $j_1 = -1.8635$ ,  $j_2 = 0.3523$ ,  $j_3 = -0.00676$ ; the approximation error is less than 0.00015 in the absolute value.

Thus, the relations (16) and (19) together with the approximate expressions (34), (35), and (36) completely determine the integral characteristics of the system. They establish relationships between the following quantities: the applied potential difference  $V$ , the emission current  $J$ , and the cone half-angle  $\alpha$ . This will allow us to compare our theoretical calculations with available experimental data in the next Section.

### III. COMPARISON WITH EXPERIMENTAL DATA

In order to compare the results of our calculations with experimental data, we assume that the control parameter of the model  $\Phi_L$  is directly proportional to the potential difference  $U$  applied to the interelectrode space, i.e.,

$$\Phi_L = \kappa U, \quad (37)$$

where the proportionality coefficient  $\kappa$  is determined by constructional features of an experimental facility and does not depend on the emission current. Then, after switching to dimensional quantities, the expressions (16) and (19) become

$$U = \left( \frac{2\sigma}{\varepsilon_0} \right)^{1/2} \frac{\sqrt{L(\alpha) \cot \alpha}}{\kappa E(\alpha)}, \quad (38)$$

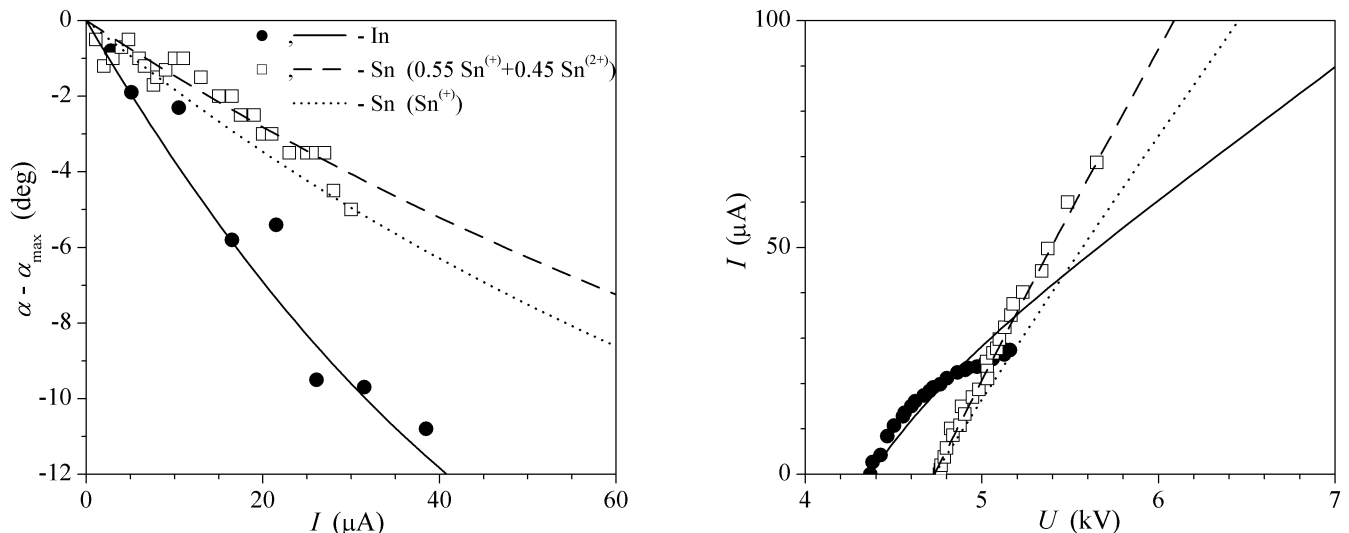


FIG. 7: The change in the cone half-angle versus the emission current (left) and the current-voltage characteristics (right) for indium and tin liquid-metal sources. The points correspond to the experimental data of [14, 17] and the lines to the theory; the solid line corresponds to indium, the dashed line to tin, and the dotted line to tin under the condition of the emission of singly-charged ions  $\text{Sn}^{(+)}$  only.

$$I = \varepsilon_0 \left( \frac{2q}{m} \right)^{1/2} F(\alpha) (\kappa U)^{3/2}. \quad (39)$$

Here we take into account that the characteristic size  $L$  of the top part of the infinite model cone (the electric current from this part of the cone is identified with the emission current from the experimentally observed conical spike) can depend on the value of the emission current and, as a consequence, on the angle  $\alpha$ .

The relations (38) and (39) together with the approximate formulas (34), (35) or (34), (36) allow one to determine the free parameters of the model, namely, the characteristic size of the cone  $L(\alpha)$  and the coefficient  $\kappa$  characterizing the electric field distribution in the experimental facilities, from the available experimental data on current-voltage and current-angle dependencies for liquid-metal ion sources. We have used data for emission into vacuum from liquid indium [14], gallium [15], tin [17], and also from liquid alloys Au+Si [16], Co+Ge [18], and Au+Ge [19]. In our calculations we have taken the following values of the surface tension:  $\sigma = 0.572$  N/m (In, [17]), 0.735 N/m (Ga, [17]), 0.560 N/m (Sn, [17]), 2.20 N/m (Au+Si, [19]), 1.84 N/m (Co+Ge, [18]), and 1.62 N/m (Au+Ge, [19]). The angular dependence of  $L$  was approximated by the two-parameter function

$$L(\alpha) = L_c + (L_T - L_c) \left( \frac{\alpha - \alpha_c}{\alpha_T - \alpha_c} \right)^2, \quad (40)$$

where  $L_T$  and  $L_c$  are parameters. It should be noted that the maximum half-angle  $\alpha_{\max}$ , corresponding to zero emission current in the experiments [14–19], slightly differs from the Taylor angle  $\alpha_T$ . Then, for comparison with the theory, the experimentally observed values of  $\alpha$  have been corrected by  $\alpha_T - \alpha_{\max}$ .

Due to its physical properties (low temperature of melting, low pressure of saturated vapor, primarily single ionization in the emission processes), gallium is the most convenient and reliable metal for investigating the operation of liquid-metal ion sources [3]. In the work [15] the gallium ion sources, including a tungsten needles with tip radius  $R_t = 2 \mu\text{m}$  and  $R_t = 20 \mu\text{m}$ , were investigated. As a result of treating data on the current-voltage characteristics and geometry of the observed structures on the surface of liquid gallium, presented in [15], we obtain:  $\kappa = 0.0905$ ,  $L_T = 0.65 \mu\text{m}$ ,  $L_c = 0.84 \mu\text{m}$  ( $R_t = 2 \mu\text{m}$ );  $\kappa = 0.076$ ,  $L_T = 0.84 \mu\text{m}$ ,  $L_c = 0.84 \mu\text{m}$  ( $R_t = 20 \mu\text{m}$ ). The achieved quality of describing the experimental data is demonstrated in Fig. 6. Application of a sharper needle (with  $R_t = 2 \mu\text{m}$ ) provides a stronger focusing of the electric field that corresponds to a larger value of the coefficient  $\kappa$  and, consequently, to a smaller value of the threshold potential difference (see Fig. 6). On the other hand, a small initial radius of curvature probably begins to “constrict” the developing cone; the value of  $L_T$  corresponding to  $R_t = 2 \mu\text{m}$  is somewhat smaller than for  $R_t = 20 \mu\text{m}$ . According to the relations (38) and (39), smaller size of the cone leads to faster change of the cone half-angle with increase in emission current, all other parameters (the surface tension coefficient, the mass and charge of emitted particles) being the same (see Fig. 6). Note that the obtained values of  $L_T$  are comparable with the size of the experimentally observed cones (they are of the order of  $1 \mu\text{m}$ ).

Fig. 7 shows the current-voltage and current-angle dependencies for the conical spikes observed at the surface of liquid indium [14] and tin [17]. Probably, the strongly nonlinear character of the current-voltage dependence for indium is an experimental error [14]. In later publications

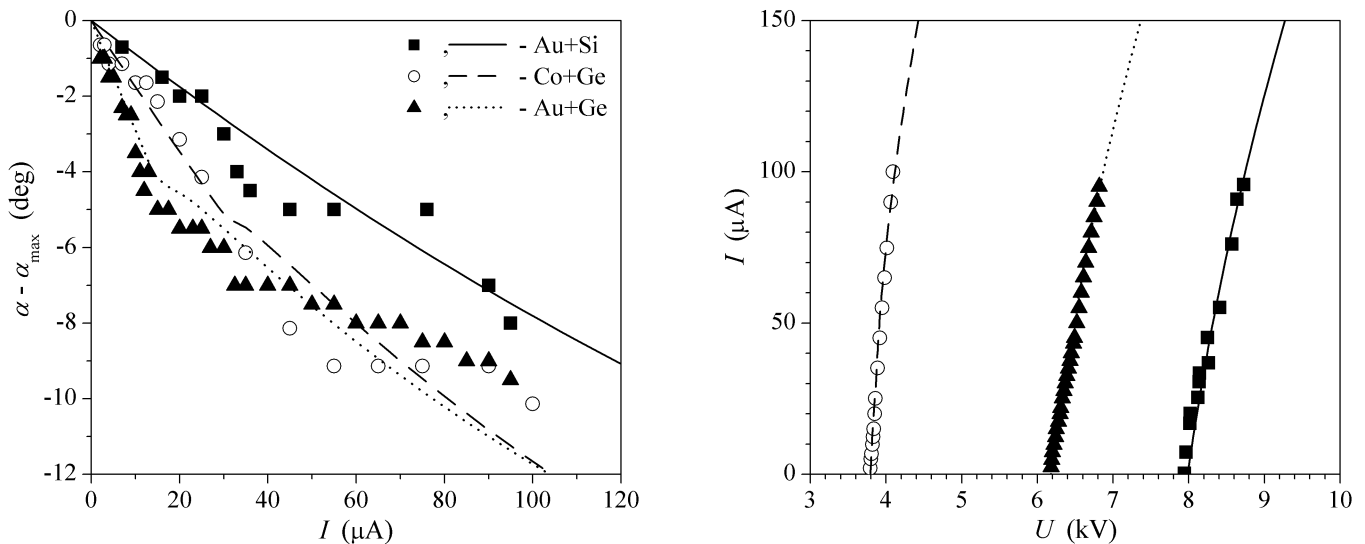


FIG. 8: The change in the cone half-angle versus the emission current (left) and the current-voltage characteristics (right) for Au+Si [16], Co+Ge [18], and Au+Ge [19] alloy liquid-metal ion sources. The points correspond to the experimental data and the lines to the theory.

[18, 19] the same authors approximate this dependence by a linear function; its slope is approximately the same as for the corresponding theoretical curve in Fig. 7.

It has been noted in [17] that both singly-charged ions  $\text{Sn}^{(+)}$  and doubly-charged ions  $\text{Sn}^{(2+)}$  are emitted from the surface of tin. The fraction of doubly-charged ions is  $x_2 = N_2/(N_1 + N_2) \simeq 45\%$  [19]. It is easy to verify that the relations obtained above are applicable for a flow consisting of  $k$  different types of particles. The only necessary modification refers to the expression for total current (39). We should apply the following change:

$$\sqrt{\frac{2q}{m}} \rightarrow \sum_{i=1}^k \frac{q_i x_i}{Q} \sqrt{\frac{2q_i}{m_i}}, \quad Q = \sum_{i=1}^k q_i x_i, \quad (41)$$

where  $q_i$ ,  $m_i$ , and  $x_i$  are the charge, mass, and relative fraction of particles of  $i$ -type. So, for the case of tin ( $q_2 = 2q_1 = 2e$ ,  $m_2 = m_1 = m$ ), the expression (39) transforms into

$$I = \frac{1 + (2\sqrt{2} - 1)x_2}{1 + x_2} \varepsilon_0 \left(\frac{2e}{m}\right)^{1/2} F(\alpha) (\kappa U)^{3/2}, \quad (42)$$

where  $e$  is the elementary charge. Indium ions are emitted in the singly-charged state  $\text{In}^{(+)}$  [19], so that such modification is not required for an indium liquid-metal ion source. The theoretical curves presented in Fig. 7 correspond to the following values of the parameters:  $\kappa = 0.0495$ ,  $L_T = 0.4 \mu\text{m}$ ,  $L_c = 0.3 \mu\text{m}$  (In);  $\kappa = 0.075$ ,  $L_T = 1.1 \mu\text{m}$ ,  $L_c = 0.78 \mu\text{m}$  (Sn).

Indium and tin have close atomic weights and surface tension coefficients. In this connection, a sharp distinction between the dependences  $I(U)$  and  $\alpha(I)$  corresponding to these metals is surprising [17]. One of the likely reasons of the different behavior of indium and tin is the

presence of a large amount of ions  $\text{Sn}^{2+}$  in the experiments [17]. Ions with larger charge numbers move faster away from the electrode and, as a consequence, provide less screening effect. Therefore, an increase in the voltage is accompanied by a larger increase in the emission current and by a relatively slow change in the cone shape. The dependences  $I(U)$  and  $\alpha(I)$ , corresponding to the assumptions that only the singly-charged ions  $\text{Sn}^{(+)}$  are emitted from liquid tin and the parameters  $\kappa$ ,  $L_T$ , and  $L_c$  are fixed, are shown in Fig. 7 by the dotted line. One can see that considering only singly-charged ions slightly approaches the model characteristics of liquid-metal emitters based on liquid tin and indium. However, the initial difference between the curves is too large and cannot be explained only by the presence of ions  $\text{Sn}^{(2+)}$ .

Another reason of the behavior difference between liquid-metal ion sources is in the conditions of experimental studies [14] and [17]. The theoretical model presented in this work points to the essential difference between the characteristic sizes  $L_T$  of the cones. One can assume that the developing cone was “constricted” by the small size of the tip of a tungsten needle in the experiment with indium ( $R_t = 1.0 \mu\text{m}$  according to [14]). Although the value of the tip radius  $R_t = 4 \mu\text{m}$  for the experiments with indium was indicated in the subsequent paper [19], it was measured with the help of the image of the liquid surface instead of the needle. The above analysis of gallium emitters with different needles shows that the “constriction” effect becomes appreciable if  $R_t \leq 2 \mu\text{m}$ .

Finally, Fig. 8 shows the dependencies  $I(U)$  and  $\alpha(I)$  for liquid alloys Au+Si [16], Co+Ge [18], and Au+Ge [19] that correspond to the model coefficients  $\kappa = 0.084$ ,  $L_T = 1.0 \mu\text{m}$ ,  $L_c = 0.45 \mu\text{m}$  (Au+Si);  $\kappa = 0.084$ ,  $L_T = 0.27 \mu\text{m}$ ,  $L_c = 0.08 \mu\text{m}$  (Co+Ge);  $\kappa = 0.051$ ,  $L_T = 0.30 \mu\text{m}$ ,  $L_c = 0.10 \mu\text{m}$  (Au+Ge). Theory and ob-

servations are in rather good agreement only for Au+Si from the above-listed alloys. The alloys containing germanium are distinguished by the presence of breaks on the experimental curves  $\alpha(I)$ . Such a behavior cannot be described in the framework of the proposed model. The anomalous character of the dependence  $\alpha(I)$  can be caused by changing properties of charged particles flow. So, “freezing” of the cone angle along with the continuing growth of the emission current, which is characteristic for the mentioned alloys (see Fig. 8), allows us to suppose that, from some point, the average ratio of mass and charge densities over the flow essentially decreases. Unfortunately, the experimental works [18, 19] does not include information about changes in the mass/charge ratio with the emission current. In Fig. 8 the theoretical curves are obtained under the assumption that the intensive emission of doubly-charged germanium ions  $\text{Ge}^{(2+)}$  starts with some value of the applied potential difference,  $U_1$  (or current,  $I_1$ ). The quantities  $U_1$ ,  $I_1$  are of the order of 3.87 kV, 30 mA for the alloy Co+Ge, and 6.3 kV, 15 mA for Au+Ge. In both cases, the potential drop is  $\Phi_L = \kappa U \simeq 0.32$  kV at the distance of the order of the cone size ( $R = L$ ).

### Conclusion

In the present paper we have developed the self-consistent model describing how the space charge near the emitting cone apex affects its shape. Our approach is based on the self-similar reduction of the equations, which govern the spatial distributions of the electric field, ion velocity field, and particle concentration, to the system of ordinary differential equations. As a result of numerical solution of this system, the conditions of the mutual compensation of the capillary and electrostatic forces on the conic surface of a liquid-metal anode have

been obtained. This allows us to find the dependences of the cone angle and emission current on the applied potential difference. They correctly represent the main features of the operation of a liquid-metal ion source. A comparison was made between the developed theoretical model and available experimental data for emission from pure gallium, indium, tin, or from alloys Au+Si, Co+Ge, and Au+Ge. Basing on our theoretical results, we have proposed explanations for some specific features of the emissive behavior of these systems. So, the difference in behavior between indium and tin having close characteristics (the coefficient of surface tension, the mass/charge ratio) is probably related with the presence of doubly-charged ions  $\text{Sn}^{(2+)}$  for tin emission and with use of a sharper tungsten needle in the experiments with indium.

In conclusion, let us note once again that the developed model does not pretend to describe all aspects of operation of liquid-metal ion sources. In particular, the consideration of the jet-like protrusion at the cone vertex, from where the vast majority of ions are evaporated, remains beyond the scope of the model. The self-similar solutions used above describe LMIS operation in terms of the averaged characteristics ( $\alpha$ ,  $I$ , and  $U$ ) only.

### Acknowledgments

The study was performed within the framework of the Program of Interdisciplinary Projects between the Ural Division and Siberian Branch of the Russian Academy of Sciences and the Program “Basic Problems of Nonlinear Dynamics” of the Presidium of the Russian Academy of Sciences. It was financially supported by the Russian Foundation for Basic Research (project 07-02-96035), by the Presidential Program of Grants in Science (project MD-2553.2007.2), and by the Dynasty Foundation.

- 
- [1] J. Zeleny, Phys. Rev. **10**, 1 (1917).
  - [2] G. I. Taylor, Proc. R. Soc. A **280**, 383 (1964).
  - [3] R. G. Forbes, Vacuum **48**, 85 (1997).
  - [4] L. Oddershede and S. R. Nagel, Phys. Rev. Lett. **85**, 1234 (2000).
  - [5] N. M. Zubarev, JETP Lett. **73**, 544 (2001).
  - [6] N. M. Zubarev, Phys. Rev. E **65**, 055301(R) (2002).
  - [7] V. G. Suvorov and N. M. Zubarev, J. Phys. D: Appl. Phys. **37**, 289 (2004).
  - [8] R. Gormer, Appl. Phys. **19**, 365 (1979).
  - [9] N. K. Kang and L. W. Swanson, Appl. Phys. A **30**, 95 (1983).
  - [10] D. R. Kingham and L. W. Swanson, Appl. Phys. A **34**, 123 (1984).
  - [11] G. S. Cho, Y. Seo, and S. O. Kang, J. Appl. Phys. **72**, 5892 (1992).
  - [12] P. Wang, S. Maheshwari, and H.-C. Chang, Phys. Rev. Lett. **96**, 254502 (2006).
  - [13] G. I. Taylor, Proc. R. Soc. London **291**, 145 (1966).
  - [14] B. Praprotnik, W. Driesel, C. Deitzsch, and H. Neidrig, Surf. Sci. **314**, 353 (1994).
  - [15] W. Driesel, C. Dietzsch, H. Niedrig, and B. Praprotnik, Ultramicroscopy **57**, 45 (1995).
  - [16] W. Driesel, C. Dietzsch, and R. Mühle, J. Phys. D: Appl. Phys. **28**, 787 (1995).
  - [17] W. Driesel and C. Dietzsch, Appl. Surf. Sci. **93**, 179 (1996).
  - [18] W. Driesel, C. Dietzsch, E. Hesse, L. Bischoff, and J. Teichert, J. Vac. Sci. Technol. B **14**, 1621 (1996).
  - [19] W. Driesel, C. Dietzsch, and R. Mühle, J. Vac. Sci. Technol. B **14**, 3367 (1996).
  - [20] C. D. Child, Phys. Rev. **32**, 492 (1911).
  - [21] I. Langmuir, Phys. Rev. **2**, 450 (1913).
  - [22] G. L. R. Mair, J. Phys. D: Appl. Phys. **17**, 2323 (1984).
  - [23] G. L. R. Mair and R. G. Forbes, J. Phys. D: Appl. Phys. **24**, 2217 (1991).
  - [24] G. L. R. Mair and R. G. Forbes, Surf. Sci. **266**, 180 (1992).

- [25] P. T. Kirstein, G. S. Kino, and W. E. Waters, *Space-Charge Flow* (McGraw-Hill, New York, 1967).
- [26] J. M. Finn, T. M. Antonsen, and W. M. Manheimer, *IEEE Trans. Plasma Sci.* **16**, 281 (1988).
- [27] G. S. Boltachev and N. M. Zubarev, *Europhys. Lett.* **76**, 36 (2006).
- [28] L. Landau and E. Lifshitz, *Course of Theoretical Physics, vol. 6: Fluid Mechanics* (Pergamon, Oxford, 1987).
- [29] A. M. Ganan-Calvo, *Phys. Rev. L* **79**, 217 (1997).
- [30] A. Barrero, A. M. Ganan-Calvo, J. Davila, A. Palacio, and E. Gomez-Gonzalez, *Phys. Rev. E* **58**, 7309 (1998).
- [31] A. Hirabayashi and J. F. de la Mora, *International Journal of Mass Spectrometry and Ion Processes* **175**, 277 (1998).
- [32] E. W. Muller, *Phys. Rev.* **102**, 618 (1956).